applied sciences

MDPI

Article

Estimating Full-Coverage $PM_{2.5}$ Concentrations Based on Himawari-8 and NAQPMS Data over Sichuan-Chongqing

Qiaolin Zeng [1,2,3], Hao Zhu [1,2], Yanghua Gao [1,2,*], Tianshou Xie [3], Sizhu Liu [3] and Liangfu Chen [4]

[1] Chongqing Institute of Meteorological Sciences, Chongqing 401147, China; zengql@cqupt.edu.cn (Q.Z.); s180201040@stu.cqupt.edu.cn (H.Z.)
[2] Chongqing Engineering Research Center of Agrometeorology and Satellite Remote Sensing, Chongqing 401147, China
[3] The College of Computer Science and Technology, Chongqing University of Posts and Telecommunications, Chongqing 400065, China; s200231036@stu.cqupt.edu.cn (T.X.); liusz@cqupt.edu.cn (S.L.)
[4] The Aerospace Information Research Institute, Chinese Academy of Sciences, Beijing 100094, China; chenlf@radi.ac.cn
* Correspondence: yanghuagaocq@gmail.com

Abstract: Fine particulate matter ($PM_{2.5}$) has attracted extensive attention due to its harmful effects on humans and the environment. The sparse ground-based air monitoring stations limit their application for scientific research, while aerosol optical depth (AOD) by remote sensing satellite technology retrieval can reflect air quality on a large scale and thus compensate for the shortcomings of ground-based measurements. In this study, the elaborate vertical-humidity method was used to estimate $PM_{2.5}$ with the spatial resolution 1 km and the temporal resolution 1 hour. For vertical correction, the scale height of aerosols (H_a) was introduced based on the relationship between the visibility data and extinction coefficient of meteorological observations to correct the AOD of the Advance Himawari Imager (AHI) onboard the Himawari-8 satellite. The hygroscopic growth factor (f(RH)) was fitted site-by-site and month by month (1–12 months). Meanwhile, the spatial distribution of the fitted coefficients can be obtained by interpolation assuming that the aerosol properties vary smoothly on a regional scale. The inverse distance weighted (IDW) method was performed to construct the hygroscopic correction factor grid for humidity correction so as to estimate the $PM_{2.5}$ concentrations in Sichuan and Chongqing from 09:00 to 16:00 in 2017–2018. The results indicate that the correlation between "dry" extinction coefficient and $PM_{2.5}$ is slightly improved compared to the correlation between AOD and $PM_{2.5}$, with r coefficient values increasing from 0.12–0.45 to 0.32–0.69. The r of hour-by-hour verification is between 0.69 and 0.85, and the accuracy of the afternoon is higher than that of the morning. Due to the missing rate of AOD in the southwest is very high, this study utilized inverse variance weighting (IVW) gap-filling method combine satellite estimation $PM_{2.5}$ and the nested air-quality prediction modeling system (NAQPMS) simulation data to obtain the full-coverage hourly $PM_{2.5}$ concentration and analyze a pollution process in the fall and winter.

Keywords: Himawari-8 AOD; vertical correction; humidity correction; NAQPMS; IVW

Citation: Zeng, Q.; Zhu, H.; Gao, Y.; Xie, T.; Liu, S.; Chen, L. Estimating Full-Coverage $PM_{2.5}$ Concentrations Based on Himawari-8 and NAQPMS Data over Sichuan-Chongqing. *Appl. Sci.* **2022**, *12*, 7065. https://doi.org/10.3390/app12147065

Academic Editors: Antoaneta Ene and Claudia Stihi

Received: 13 June 2022
Accepted: 5 July 2022
Published: 13 July 2022

1. Introduction

The $PM_{2.5}$, as known as fine particulate matter, denotes particulate matter with an aerodynamic diameter less than 2.5 μm. $PM_{2.5}$ has raised significant public concerns over the past decades because of its adverse effects on human health [1]. Studies have shown that people who exposed to $PM_{2.5}$ for long periods of time are more likely to suffer from respiratory and cardiovascular diseases and even die prematurely [2,3]. Therefore, long-term continuous regional $PM_{2.5}$ concentration monitoring is important for the assessment of various haze impacts. To monitor air pollutants, China started to develop a ground-based monitoring network at the end of 2012, which has covered major cities by now. The ground-based monitoring network can grasp the real-time information of $PM_{2.5}$ concentration

overtime at the observation sites with high accuracy, but it is difficult to support the assessment of regional haze impact due to the inability to accurately represent non-site regional concentrations. Meanwhile, the cost of site maintenance is high and the distribution is uneven with most located in urban centers. To overcome these limitations, the use of satellite remote sensing technology to derive the spatial and temporal distribution characteristics of $PM_{2.5}$ was proposed [4], due to its advantages such as wide spatial coverage and long time series [5,6].

The AOD retrieved by satellite is a measure of the integration of the extinction coefficient of the medium between satellite remote sensing and the ground in the vertical direction [7], which cannot directly represent the ground-level $PM_{2.5}$. Therefore, various methods have been proposed to represent the relationship between AOD and $PM_{2.5}$, and obtain the near-ground $PM_{2.5}$ concentration. Up to now, the main methods for estimating $PM_{2.5}$ concentration using AOD are scale factor methods, semi-empirical formula methods, statistical model methods, and machine learning methods. The scale factor method simulates the scale coefficient between $PM_{2.5}$ and AOD by atmospheric radiative transfer model and then multiplies the coefficient by the AOD obtained from satellite retrieval, which does not involve ground-based monitoring data and is conducive to estimating $PM_{2.5}$ concentration during the period when there is no ground-based monitoring station, but the estimation accuracy is low [8–10]. The semi-empirical formula method is based on the physical properties between AOD and $PM_{2.5}$ such as humidity and vertical profile features of AOD [11–15]. However, it is difficult to fully express the relationship between $PM_{2.5}$ and AOD by a simple function due to its complex physical mechanism, while some parameters in the semi-empirical formula are not easily accessible, which limits the extension of this method. The statistical model method evolved from the initial linear model (e.g., linear mixed-effect regression, LME) [16,17] to the nonlinear regression model (e.g., generalized additive model, GAM; geographically and temporally weighted regression, GTWR) [18–20]. Some researches improve the accuracy of the model by introducing meteorology, topography, land use and other relevant parameters [21,22], but the nonlinear relationship between the factors still cannot be fully expressed. Machine learning algorithms have significant advantages over statistical models for classification and prediction [23], and a variety of models are widely used for $PM_{2.5}$ estimation, e.g., random forest (RF) [24,25], Deep Neural Networks (DNN) [26,27], Capsule Networks (CapsNet) [28], space-time extremely randomized trees (STEM) [29]. Machine learning methods have the advantage of expressing nonlinear relationships between large data and achieve excellent results in estimation accuracy compared with other methods but ignore the physical characteristics between AOD and $PM_{2.5}$. As the relationship between AOD and $PM_{2.5}$ varies greatly from region to region, moment to moment, and season to season [30,31], most studies that used a single machine learning method to estimate $PM_{2.5}$ concentrations in a large area have some shortcomings in spatial distribution. Meanwhile, the accuracy of the estimation using machine learning methods is related to the training samples.

Meanwhile, there is still a huge challenge in estimating regional $PM_{2.5}$ concentrations using AOD, which is missing AOD retrievals caused by cloud cover and bright surfaces (desert or snow) [32,33]. Different methods are proposed for addressing missing AOD retrievals, such as kriging interpolation [34], machine learning methods to combine chemical transport models such as the Community Multi-scale Air Quality Model (CMAQ), Modern-Era Retrospective Analysis for Research and Applications-version 2 (MERRA-2) to simulate AOD or $PM_{2.5}$ with complete spatial and temporal coverage. For example, Sun et al. combined Multi-angle Implementation of Atmospheric Correction (MAIAC) AOD, AHI AOD, and meteorological data to obtain 24 h full-coverage $PM_{2.5}$ concentrations in Beijing [35]. Li et al. used residual networks for the downscaling fusion of MERRA-2 and MAIAC AOD to obtain full-coverage of $PM_{2.5}$ concentrations in the California [36]. Chen et al. used AQUA and TERRA AOD to perform linear regression firstly, and then combined with Copernicus Atmosphere Monitoring Service (CAMS) AOD, using a self-adaptive deep neural network (SADNN) to estimate regional full-coverage $PM_{2.5}$ in China [37]. Bai et al.

performed ten different fusion strategies for comparison to obtaining full-coverage $PM_{2.5}$ concentrations using the classical RF model [38].

Due to the unique climatic conditions in the Sichuan and Chongqing regions, where the air pollution is heavier but with more cloud coverage in autumn and winter, and less cloud coverage but relatively better air quality in spring and summer. As well know, machine learning method is relation with training samples, the training samples in the special area of the study may not truly represent the distribution of $PM_{2.5}$ long-time series. Thus, we proposed the elaborate Vertical-Humidity correction method to estimate $PM_{2.5}$ concentrations in areas of Sichuan and Chongqing (the scope of the study mainly includes the Sichuan area except Ganzi, Aba, Liangshan, and Panzhihua, and the main urban area of Chongqing). Meanwhile, to make up for the missing data of $PM_{2.5}$ retrieved by satellite, we combine satellite and NAQPMS data to obtain full-coverage $PM_{2.5}$ concentration over Sichuan and Chongqing. The main research of this study is as follows:

(1) Considering the complex topography and meteorological conditions in Sichuan and Chongqing, the scale height of aerosols (H_a) was introduced for the vertical correction of regional AOD. For humidity correction, five different stations were selected for the analysis of the fitted curves and f(90%), and the results showed that the hygroscopic correction factors varied greatly in different months and stations, so the data in the study area were fitted site by site and month by month to construct a grid of hygroscopic correction factors.
(2) The hourly $PM_{2.5}$ concentrations in the study area from 09:00 to 16:00 were estimated using the AHI AOD data based on the constructed hygroscopic correction factors grid, and the accuracy was verified.
(3) Considering the frequent cloud coverage in Sichuan and Chongqing regions and the existence of gaps in the satellite retrieval $PM_{2.5}$, we adopt inverse variance weighting (IVW) for effective fusion with the help of NAQPMS data to finally obtain $PM_{2.5}$ concentrations with seamless coverage and effectively analyze the processes of pollutant aggregation, migration, and dissipation in this place.

2. Materials and Methods

The study area we selected mainly includes Sichuan Province (except Ganzi, Aba, Liangshan, and Panzhihua) and the main urban area of Chongqing (Figure 1), which located in southwest China, with regional elevations ranging from 400–5000 m [39]. The study area is influenced by the Qinghai-Tibet Plateau to form high humidity and low wind speed atmospheric conditions, which are not conducive to pollution transmission and are prone to haze with the wide range and long duration leading to heavy pollution. Additionally, the population of the region is about 100 million, and a large amount of industrial, traffic, and anthropogenic emissions of pollutants leads to frequent heavy pollution weather [40].

2.1. Data

2.1.1. Ground-Level $PM_{2.5}$ Measurements

Ground measured hourly $PM_{2.5}$ concentration data in 2017 and 2018 were obtained from the China National Environmental Monitoring Center (CNEMC) (http://106.37.208.233:20035/, accessed on 12 June 2022), Department of Ecology and Environment of Sichuan Province, and Chongqing Environmental Monitoring Center, including CNEMC stations, Sichuan stations, and Chongqing stations. For every three hours of data, $PM_{2.5}$ concentration values below the 3% quantile or above the 97% quantile are not included in the calculation.

2.1.2. Himawari-8 AHI/AOD Data

Himawari-8 is a second-generation geostationary meteorological satellite of Japan Meteorological Agency (JMA), which was successfully launched in October 2014 and officially put into operation in July 2015. Himawari-8 carries an AHI sensor with 16 observation channels, which includes 3 visible channels, 3 near-infrared channels, and 10 infrared

channels, of which the resolution of visible channels can reach 0.5 km, and the resolution of near-infrared and infrared channels can reach 1~2 km. This study used the AOD by the dark target algorithm retrieval with a spatial resolution of 1 km and a temporal resolution of 1 h; please refer to the literature for the detailed retrieval algorithm [41].

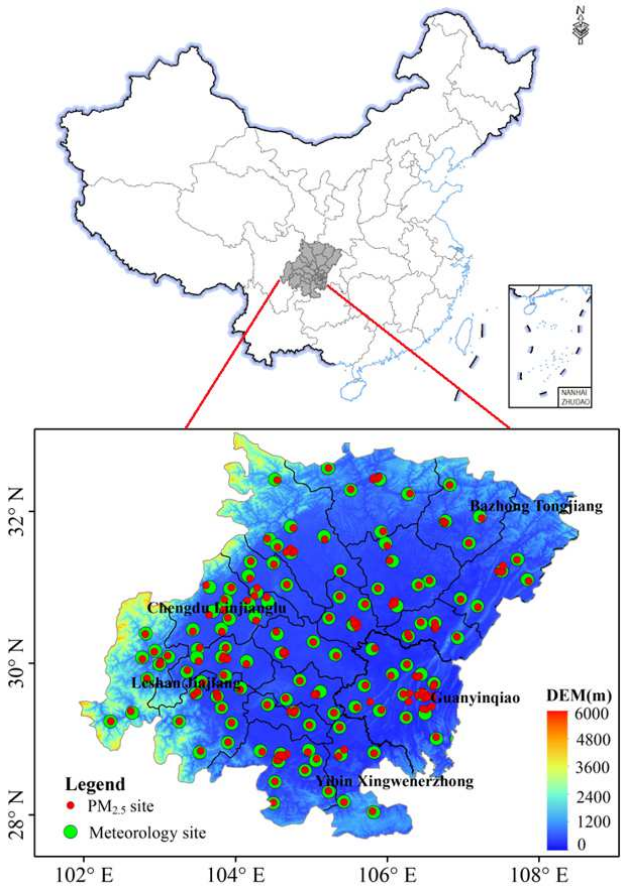

Figure 1. Location of $PM_{2.5}$ and meteorology monitoring stations in study area.

2.1.3. Meteorological Data

The meteorological data were obtained from China Meteorological Data Service Centre with a temporal resolution of 1 h, and the two main parameters utilized were visibility (VIS) and relative humidity (RH). To reduce the experimental error, the data were pre-processed as follows. (1) If the ratio of the visibility data of the current day to the data of the previous day and the next day was less than 1/3 in three consecutive days, the visibility data of that day were deleted [42]. (2) Relative humidity values greater than 98% were not involved in the statistical study. (3) To avoid affecting the aerosol hygroscopic growth fitting results, when matching environmental monitoring station data and meteorological station data, if the distance between two stations was greater than 10 km, they were not involved in the statistical study.

2.1.4. Aerosol Robotic Network (AERONET) Data

To verify the accuracy of the AHI AOD in the retrieval of this study, we downloaded the AERONET [43] level 2.0 data of 2017 and 2018 at six stations: Bamboo (25.19° N, 121.54° E), Hong Kong PolyU (22.3° N, 114.18° E), Hong Kong Sheung (22.48° N, 114.12° E), Beijing CAMS (39.93° N,116.32° E), Xiang He (39.75° N, 116.96° E), and Beijing (39.98° N, 116.38° E). The AERONET AODs were interpolated using 440 nm and 675 nm with the help of Angstrom exponential to be consistent with the AHI AOD 550 μm band [44]. During the validation process, to ensure consistency in space and time, the average value

of 3 × 3 images was calculated with AERONET sites as the center, and the average value of AERONET AOD before and after half an hour of satellite transit time was calculated, with a total of 4544 validation data. The validation comparison scatter plot is shown in Figure 2, with a high correlation coefficient value of r = 0.82 and a fit slope close to 1, RMSE = 0.38.

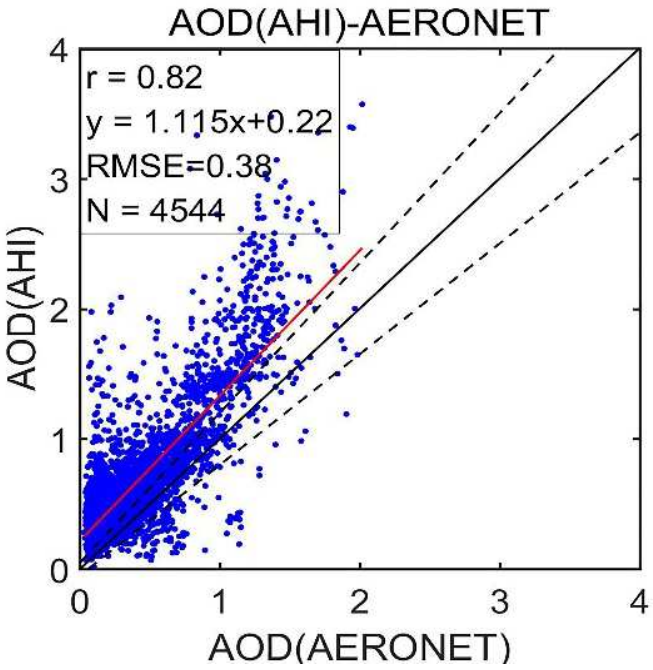

Figure 2. Scatterplot of AOD (AHI) and AOD (AERONET). The dashed, black, and red solid lines are the expected errors of ± (0.05 + 15%), 1−1 line, and linear regression of the scattered dots, respectively.

2.1.5. Nested Air Quality Prediction Modeling System (NAQPMS) Data

The simulated $PM_{2.5}$ data used in this study were obtained from the Nested Air Quality Prediction Modeling System (NAQPMS); the NAQPMS is a multiscale air-quality model developed by the Institute of Atmospheric Physics, Chinese Academy of Sciences. The NAQPMS uses a new generation of mesoscale Weather Research and Forecast (WRF) models with a resolution of 1–30 km developed by the National Center for Environmental Prediction (NCEP), the National Center for Atmospheric Research (NCAR), and other research institutions and universities [45,46]. The NAQPMS can simulate atmospheric trace gases (e.g., O_3, NO_X, SO_2, CO) and atmospheric aerosol components (e.g., sand, sea salt, sulfate, nitrate, ammonium, and carbon-containing aerosols). It has been widely used in the study of the development mechanism and transport deposition process of sand, dust, acid rain, ozone, and particulate pollution, as well as the forecast and prediction of urban air quality [47]. To be consistent with the AHI AOD resolution, the NAQPMS was resampled to 1 km by the nearest neighbor method.

2.2. Methods

AOD represents the sum of the extinction capacity of all aerosol particles in the vertical column of the atmosphere. To obtain near-ground $PM_{2.5}$, not only the near-ground extinction coefficient needs to be revised from the vertical extinction coefficient, but also the hygroscopic properties of the particles should be considered. However, the hygroscopic properties of aerosol particles vary greatly in different seasons and regions, so this study fitted the hygroscopic growth factors month by month and site by site and constructed a grid of hygroscopic correction factors by using the IDW method.

2.2.1. Vertical Correction

Assuming that the extinction coefficient of the aerosol shows a negative exponential decay in the vertical direction, the AOD can be expressed as:

$$\mathrm{AOD} = \int_0^{\infty} \sigma_a(\lambda) \times e^{-\frac{z}{H_a}} dz = \sigma_a(\lambda) \times H_a \quad (1)$$

where $\lambda = 550$ nm, z denotes the height in the vertical direction, and $\sigma_a(\lambda)$ is the near-ground extinction coefficient, which unit is m^{-1}. H_a is the scale height of aerosols. H_a can be approximately replaced by the boundary [48], the unit of which is m.

According to Koschmieder's law [49–51], the near-ground extinction coefficient $\sigma_a(\lambda)$ can be expressed by Equation (2):

$$\sigma_a(\lambda) = \frac{3.912}{\mathrm{vis}} - \frac{32\pi^3(n-1)^2}{3N\lambda^4} \quad (2)$$

where n denotes the atmospheric refractive index, and N denotes the molecular number density. At sea level, $n - 1 = 293 \times 10^{-6}$, $N = 266 \times 10^{-19}$ cm^{-3}.

Therefore, the visibility provided by the meteorological station can be used to calculate the near-ground extinction coefficient $\sigma_a(\lambda)$ and thus the corresponding H_a. Assuming that the variation of H_a is small within a certain range, this study uses IDW to interpolate H_a distribution to 1 km in the study area.

2.2.2. Relativity Correction

Based on the Mie scattering theory [11,48], the near-ground extinction coefficient of aerosols $\sigma_a(\lambda)$ can also be expressed as:

$$\sigma_a(\lambda) = \frac{3\langle Q_{ext}\rangle}{4r_{eff}\rho} \cdot PM_x \quad (3)$$

where $\langle Q_{ext}\rangle$ denotes the scattering efficiency of normalized particles, r_{eff} denotes the effective radius of the particle, ρ denotes the average density of particles, PMx denotes the mass concentration of aerosol, and all parameters are influenced by relative humidity. Assuming that the particles, particle spectrum, and density of the aerosol remain relatively constant, $\langle Q_{ext}\rangle$, r_{eff}, and ρ can be viewed as constants so that there is a certain positive relationship between $\sigma_a(\lambda)$ and PMx. According to the average mass extinction rate defined by Wang [11].

$$E_{ext} = \frac{\sigma_a(\lambda)}{PM_x} \approx E_{ext}(RH) \quad (4)$$

Since the fine particulate matter is the main contributor to aerosol extinction, here, PMx refers to particulate matter with a particle radius less than 2.5 μm, and $E_{ext}(RH)$ describes the average state of the extinction ability of particles with different properties. To quantitatively describe the hygroscopic growth characteristics of $E_{ext}(RH)$, the extinction hygroscopic growth factor of the average mass extinction rate f(RH) can be expressed as

$$f(RH) = \frac{E_{ext}(RH)}{E_{dry}} \quad (5)$$

where E_{dry} denotes the average mass extinction rate under dry conditions (RH = 40%). According to the Kotchenruther's research [52], $E_{ext}(RH)$ can be represented by Equation (6),

$$E_{ext}(RH) = a + b \times \left(\frac{RH}{100}\right)^c \quad (6)$$

where a, b, and c are coefficients fitted with RH variation, depending on the aerosol physicochemical properties. According to the above equations, the expression of $PM_{2.5}$ can be obtained as follows:

$$PM_{2.5} = \frac{\sigma_a(\lambda)}{E_{ext}(RH)} = \frac{\frac{AOD}{H_a}}{\left(a + b \times \left(\frac{RH}{100}\right)^c\right) \times E_{dry}} \quad (7)$$

Since fine particles can stay in the atmosphere for days or even weeks and can be well mixed in the atmosphere and transported over long distances to other regions, the spatial distribution of the fitted coefficients a, b, and c can be obtained by interpolation, assuming that the aerosol properties vary smoothly on a regional scale. Subsequently, assuming that the regional relative humidity varies smoothly, the distribution of relative humidity in the study area can be obtained by IDW interpolation. Finally, the $PM_{2.5}$ concentration value of each pixel can be calculated based on the AOD, H_a, relative humidity, a, b, and c in the study area.

2.2.3. IVW Fusion Method

To fill the gap in $PM_{2.5}$ estimation by satellite, we used the inverse variance weighting method (IVW), which is based on the difference between $PM_{2.5}$ estimated by satellite (NAQPMS) and ground-based $PM_{2.5}$ data, to fuse satellite data and NAQPMS data. Since the dispersion of the variance is related to the quality of the estimation (or simulation) results, by calculating the variance of the corresponding data pair, a lower weight is assigned when the variance between the estimated (simulated) results and the ground-based data is large, and when the variance is small, a higher weight is assigned [53]. The IVW method is expressed as follows:

$$PM_f = \frac{\frac{PM_{st-f}}{Var_{stm}} + \frac{PM_{model-f}}{Var_{modelm}}}{\frac{1}{Var_{stm}} + \frac{1}{Var_{modelm}}} \quad (8)$$

where PM_{st-f} and $PM_{model-f}$ denote $PM_{2.5}$ of satellite estimation and NAQPMS simulation. Var_{stm} (Var_{modelm}) is the variance of the difference between the satellite estimation (NAQPMS simulation) and the ground-based $PM_{2.5}$. PM_f is $PM_{2.5}$ concentration after fusion.

This study fused the satellite estimated $PM_{2.5}$ with the NAQPMS simulation results to obtain spatially full-coverage $PM_{2.5}$ distribution.

3. Results

3.1. The Fitting Result of $E_{ext}(RH)$ and Statists Analysis of $f(RH)$

In this study, $E_{ext}(RH)$ fitting results for five different urban sites were selected for analysis, which are Chengdu Lingjianglu (built-up area), Leshan Jiajiangxian (near the river), Yibin Xingwenerzhong (densely vegetated area), Bazhong Tongjiangzhongxue (near the river), and Chongqing Guanyinqiao (commercial area), and the fitting results are shown in Figure 3 and Figures S1–S4. In general, (1) the fitting ability of the model was strong at all five stations, with r around 0.9 at the stations of Leshan Jiajiang, Yibin Xingwen, and Chongqing Guanyinqiao; only in February, June, and December was the r less than 0.8 at the station of Bazhong Tongjiang, and the r was less than 0.8 at the station of Chengdu Linjiang only in July and August. (2) While the RH value is small, $E_{ext}(RH)$ grows slowly with RH, but the fitted curve is flat while RH > 80%, and the $E_{ext}(RH)$ shows a fast-rising trend.

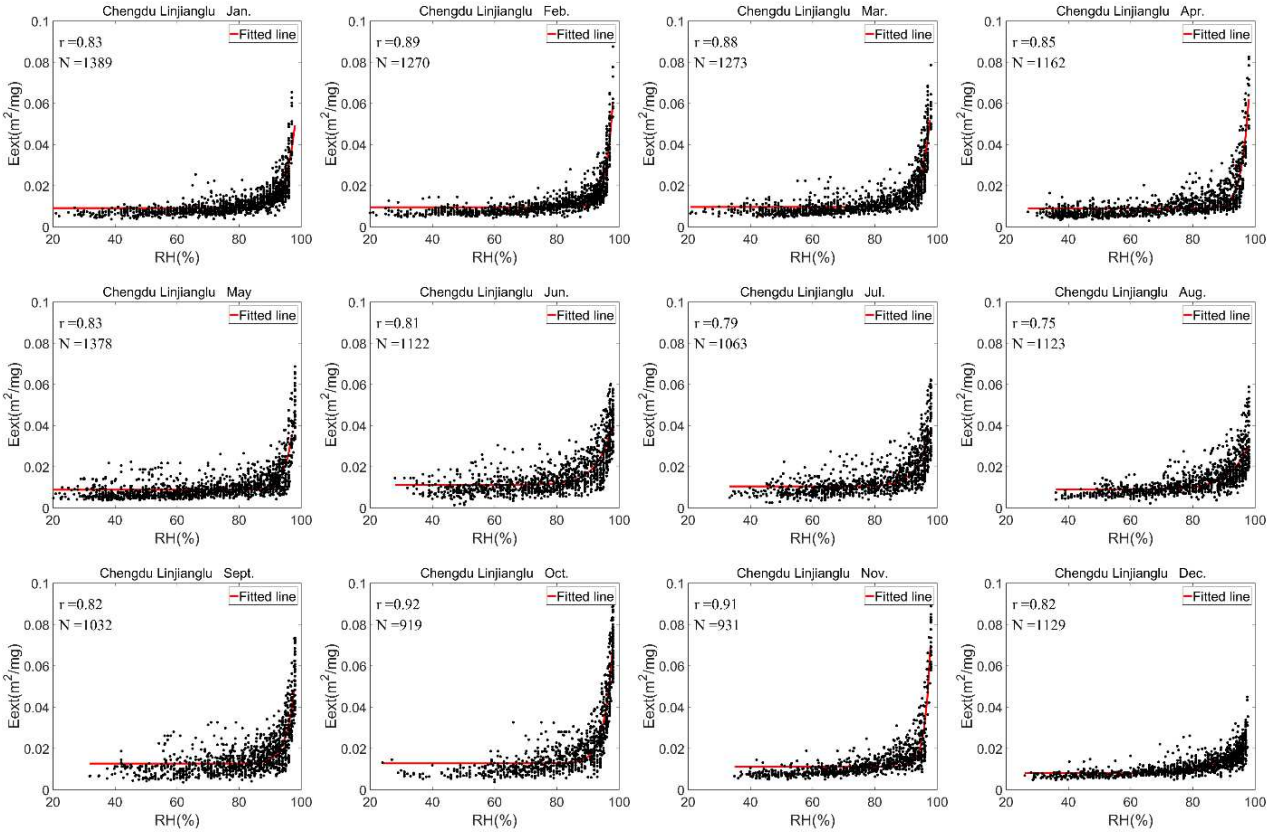

Figure 3. $E_{ext}(RH)$ fitting Chengdu Lingjianglu station. The red solid lines are fitting lines of the scattered dots.

The fitting results of the five stations have obvious differences: the fitted curve of the Chengdu Lingjianglu station is basically the same from January to December and shows a slow rise when the relative humidity is higher, indicating that the aerosol hygroscopic growth characteristics of this station are weak, and its aerosol sources and environmental conditions vary less with the season [54], which may be related to the location of the selected station in a built-up area. The differences in hygroscopic growth characteristics between the months are large at Leshan Jiajiang and Bazhong Tongjiang, which are located close to the river. The fitted curve of Leshan Jiajiang shows a slow rise from January to May but a sharp rise from June to October, indicating that the hygroscopic growth characteristics vary greatly with the seasons, and there is almost no relative humidity less than 40% in July and August. For Bazhong Tongjiang, the fitted curve shows a sharp and steep rise in all 12 months. The hygroscopic growth characteristics of Yibin Xingwen, located in a densely vegetated area, and Chongqing Guanyinqiao Station, located in a commercial area, are relatively similar, where the fitted curves both show a slow rise from January to December with no obvious deliquescence.

Using Equation (5), f(90%) from January to December was calculated for Chengdu Linjianglu, Leshan Jiajiangxian, Yibin Xingwenerzhong, Bazhong Tongjiangzhongxue, and Chongqing Guanyinqiao, respectively. The corresponding f(90%) could not be calculated because of the missing value of relative humidity less than 40% in December at Chongqing Guanyinqiao station and in July and August at Leshan Jiajiang station, as shown in Table 1. Comparison of different stations showed that the hygroscopic growth factors varied widely among stations, the variation of f(90%) at the same site in different months was large. There are 3.91 in November and 1.70 in February at Yibin Xingwenerzhong, and 5.02 in February and 1.13 in October at Leshan Jiajiangxian. The f(90%) of Chongqing Guanyinqiao is the highest (low) at 5.35 (2.46). There are small variations both Chengdu Linjianglu and Bazhong Tongjiangzhongxue stations. The f(90%) at Chongqing Guanyinqiao and Leshan

Jiajiangxian stations are significantly higher than other stations, which the reason is that the main source of aerosols in commercial areas is secondary pollutants (such as sulfates) from vehicle emissions, which are water-soluble ions with strong hygroscopic properties. Leshan Jiajiangxian site is located between the built-up area and the river, and the aerosol is relatively complex.

Table 1. Hygroscopic growth ability of f (90%) at Chengdu Linjianglu, Leshan Jiajiangxian, Yibin Xingwenerzhong, Bazhong Tongjiangzhongxue, and Chongqing Guanyinqiao.

Month	Chengdu Linjianglu	Yibin Xingwenerzhong	Leshan Jiajiangxian	Bazhong Tongjiang	Chongqing Guanyinqiao
January	1.85	1.62	3.64	1.51	2.46
February	1.58	1.70	5.02	1.65	2.51
March	1.58	2.38	4.92	1.65	2.67
April	1.57	3.52	4.59	1.45	4.85
May	1.47	2.66	4.03	1.33	3.94
June	1.70	1.92	2.44	1.46	3.78
July	2.08	1.93	-	1.85	4.78
August	2.52	1.83	-	1.21	4.64
September	1.99	2.38	3.22	1.19	5.35
October	1.20	3.52	1.13	1.41	3.27
November	1.61	3.91	3.26	1.62	5.34
December	2.22	2.57	2.68	2.14	-

3.2. Vertical and Humidity Correction on AOD

To verify that the dry extinction coefficient of AOD after vertical and humidity corrections (σ_{dry}) is useful for estimating $PM_{2.5}$ concentration, the scatter plots of AOD&$PM_{2.5}$ from 09:00 to 16:00 (Beijing time) and the σ_{dry} and $PM_{2.5}$ are shown in Figures 4 and 5. According to Figure 4, the correlation coefficient between AOD and $PM_{2.5}$ increased by hours, and the correlation coefficient ranged from 0.11 to 0.44 (the lowest correlation r = 0.11 at 9:00 and the highest correlation r = 0.44 at 16:00). The correlation between the σ_{dry} and $PM_{2.5}$ was significantly improved (Figure 5), with the highest correlation r = 0.68 at 15:00. Comparison of Figures 4 and 5 shows that the correlation between the σ_{dry} and $PM_{2.5}$ after the vertical and humidity corrections is significantly improved, which is beneficial to the estimation of $PM_{2.5}$ concentration.

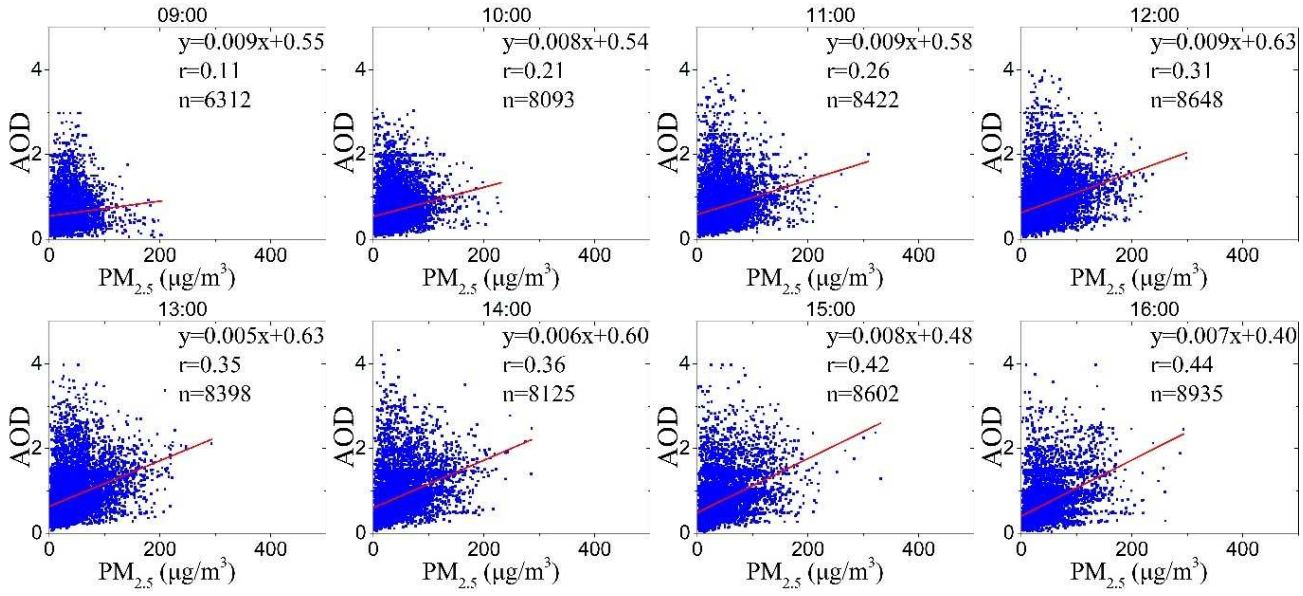

Figure 4. Scatterplot of AOD and $PM_{2.5}$ at different times (09:00–16:00) in study area.

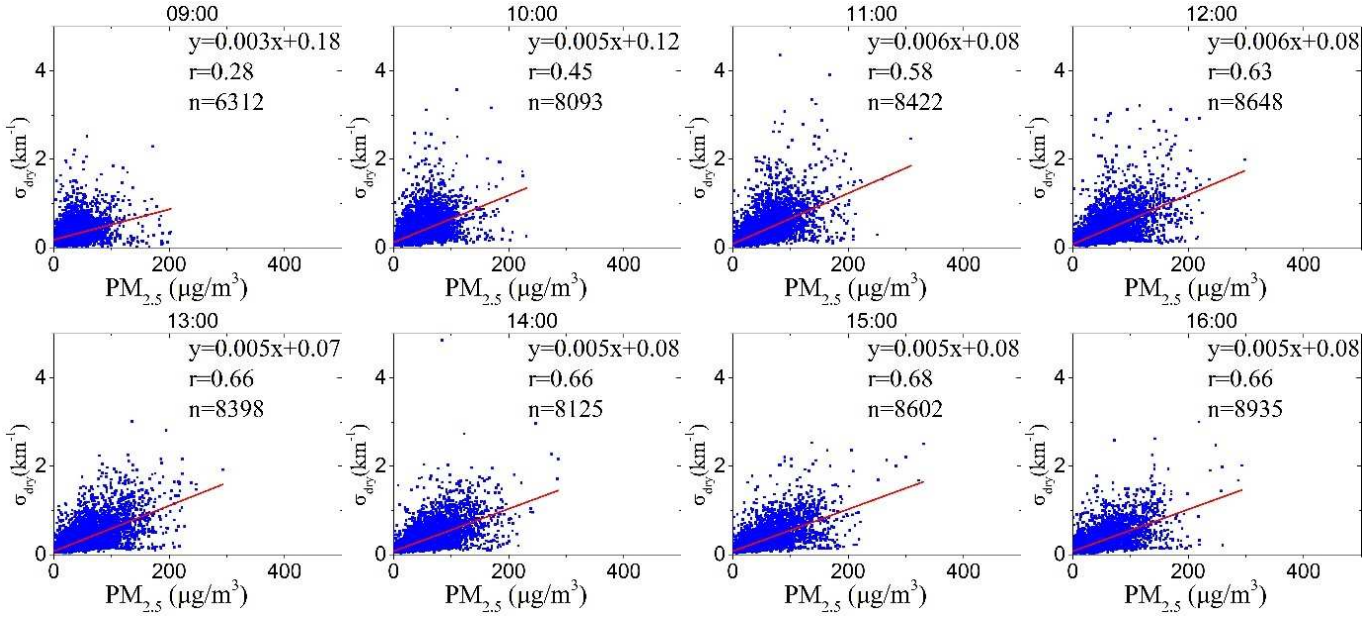

Figure 5. Scatterplot of "σ_{dry}" and $PM_{2.5}$ at different times (09:00−16:00) in study area.

3.3. The $PM_{2.5}$ of Satellite Estimation Validation

The comparison of Figures 4 and 5 shows that the correlation between σ_{dry} and $PM_{2.5}$ is significantly improved after the vertical and humidity corrections compared to that between AOD and $PM_{2.5}$, and the correlation coefficient increases from 0.11–0.44 to 0.28–0.68. The mass concentration of near-ground $PM_{2.5}$ was estimated using Equation (8), and the hour-by-hour density scatter plots of satellite estimates against ground-based observations are shown in Figure 6, where the red dashed line is the 1:1 line, and the blue dashed line is the fitted line. According to Figure 6 the correlations are all high in general, but the correlation coefficient varies more from 09:00 to 16:00 (0.69–0.85), and the correlation is significantly higher in the afternoon than in the morning, the variation of which is consistent with the study of Xu [30]. This may be caused by the following two reasons: (1) in the morning hours, when the solar azimuth is larger and the atmospheric water vapor content is higher, the sunlight passes through a longer atmospheric path to reach the ground, which affects the accuracy of the AOD retrieval, and thus the $PM_{2.5}$ estimation results may be relatively poor, especially at 09:00. (2) Particulate matter deliquesces with the increase in temperature, which may affect the results of humidity corrections [15] and thus affect the $PM_{2.5}$ estimation results. (3) In the process of vertical revision, we use the visibility to calculate the near-surface extinction coefficient ($\sigma_a(\lambda)$). The fog or high humidity conditions in the morning over the Chengdu-Chongqing regions may affect the visibility measurement, thus affecting the final $PM_{2.5}$ estimation [51]. (4) We fit this based on the monthly scale in constructing the hygroscopic correction factor grid, which may have a greater impact at 9:00 and 10:00 because of the high humidity conditions, so it is necessary to construct the hygroscopic correction factor grid for a more refined sub-hour.

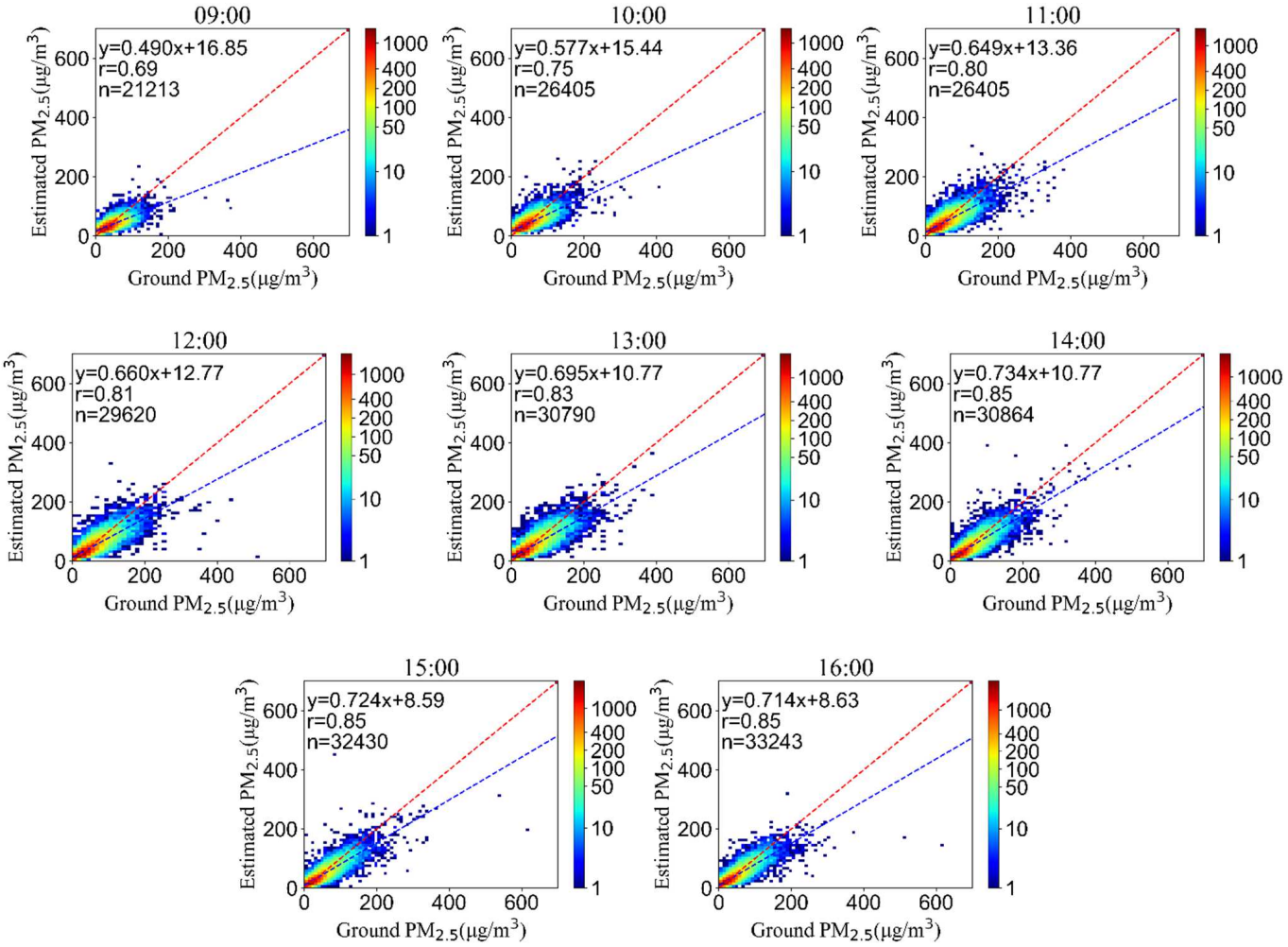

Figure 6. Scatterplot of the hourly density of $PM_{2.5}$ from satellite estimation and ground-based observation (09:00–16:00). The red and blue lines are 1:1 and fitted lines.

3.4. Application of Hourly $PM_{2.5}$ in Pollution Event Analysis

In this study, we plotted the satellite estimations (Figure 7a–d,i–l) and the satellite-NAQPMS fused $PM_{2.5}$ spatial distribution (Figure 7e–h,m–p) from 09:00 to 16:00 on 19 April 2017. According to the spatial distribution, there are gaps in the satellite estimation $PM_{2.5}$ due to the influence of cloud coverage, which cannot reflect the pollution in some regions (Figure 7a–d,i–l). The full-coverage $PM_{2.5}$ spatial distribution was obtained after the fusion of satellite and NAQPMS data to make up for the shortcomings of satellite estimation results. At 09:00, the $PM_{2.5}$ high concentration area is mainly located in the junction of Meishan, Leshan, and Zigong; at 10:00, with the transit of southeast wind, pollutants migrate to Meishan and Chengdu, while the $PM_{2.5}$ concentration of some regions increases; at 11:00, with the transit of the northeast wind, pollutants of Ziyang and Deyang area migrate with the wind and pollutants accumulate in Meishan area, making $PM_{2.5}$ concentration higher; until 16:00, the northeast area of Sichuan pollutants diffuse and migrate with the wind, making the air quality better and $PM_{2.5}$ concentration lower. However, Leshan, Meishan, and Ya'an are located in the wind accumulation area and left of the mountainous area, making pollutants accumulate and $PM_{2.5}$ concentration relatively high.

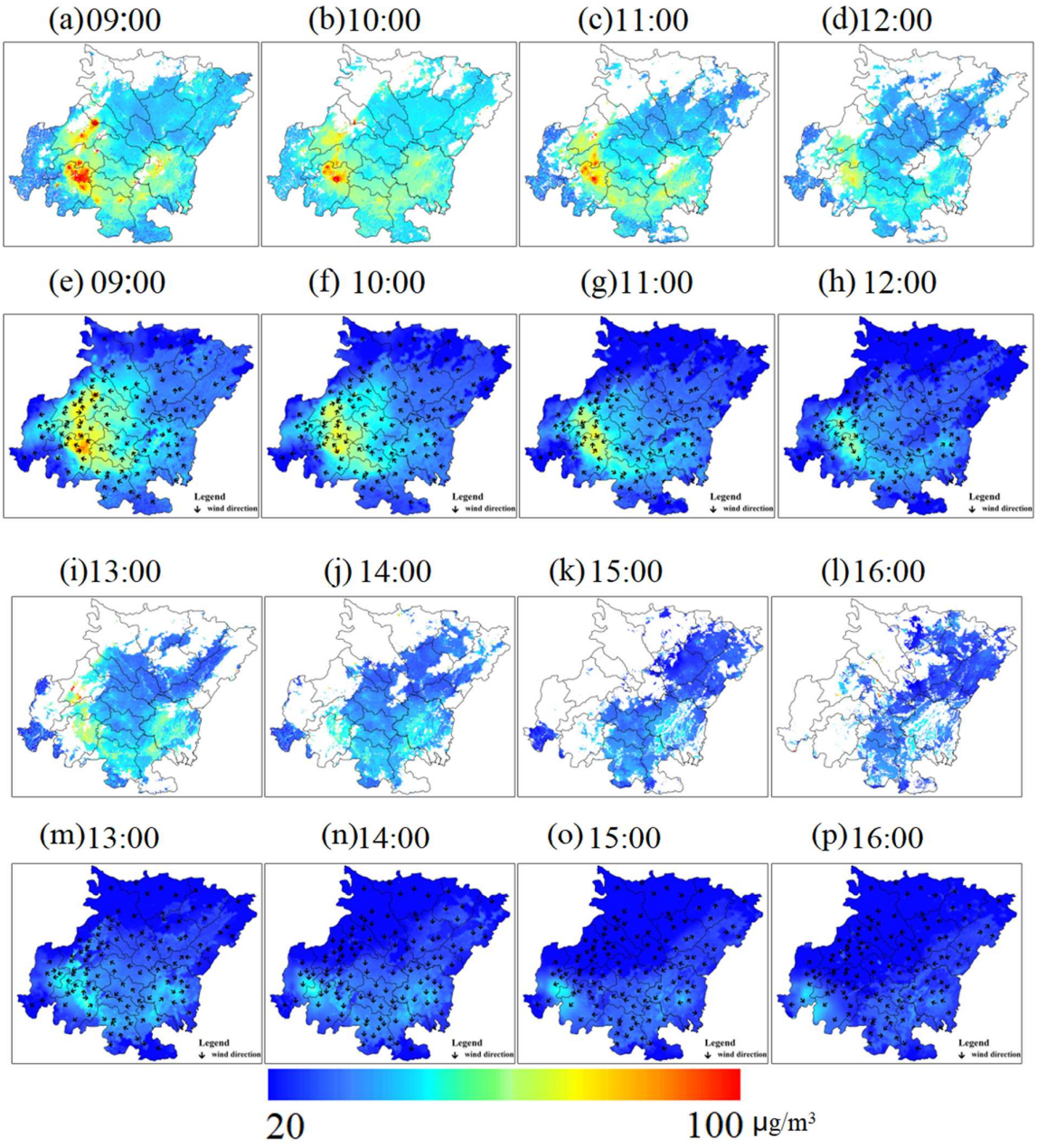

Figure 7. $PM_{2.5}$ spatial distribution on 19 April 2017 09:00–16:00. (**a**–**d**,**i**–**l**) denote satellite estimation results; (**e**–**h**,**m**–**p**) denote model and satellite fusion results. The black arrows are wind direction.

In addition, we selected the $PM_{2.5}$ pollution process from 1 to 3 November 2018, as shown in Figure 8. According to the $PM_{2.5}$ concentration distribution and migration process, it can be seen that on November 1, $PM_{2.5}$ high concentration (>100 $\mu g/m^3$) is mainly located in the junction of Suining, Ziyang, Chengdu, and Deyang at 09:00; until 16:00, pollutants gradually dissipated and high concentration region migrates around Mianyang. On 2 November, the high concentration area is located near Meishan and Chengdu at 09:00; with the diffusion of pollutants, $PM_{2.5}$ concentration gradually decreases and is mainly concentrated in Leshan at 16:00. On 3 November, pollutants migrate and gather near Yibin and Luzhou, and the whole pollution process ends by 16:00. Therefore, the results of spatial full coverage obtained by fusion can analyze the changes in pollutant migration, diffusion, and accumulation.

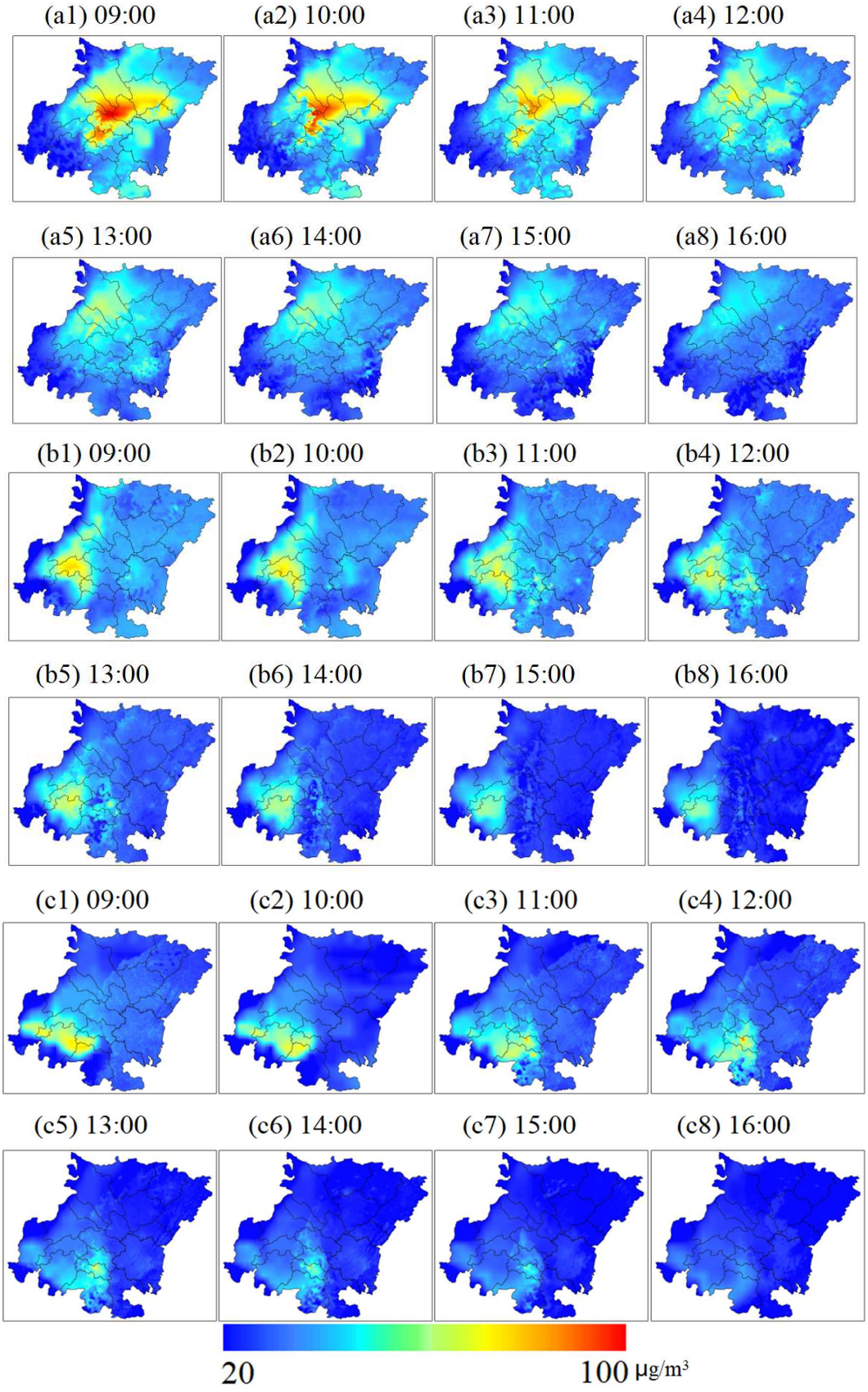

Figure 8. $PM_{2.5}$ spatial distribution on 1 to 3 November 2018 at 09:00–16:00. (**a1**–**a8**) denote 1 November; (**b1**–**b8**) denote 2 November; (**c1**–**c8**) denote 3 November.

4. Discussion

In this study, the near-ground extinction coefficient was calculated using the visibility in the vertical correction to calculate the H_a of the corresponding pixel. According to the principle of ground-based observation visibility, the near-ground extinction coefficient calculated by using Equation (2) represents the integration of the particle extinction ability in the horizontal direction, while the AOD represents the integration of the particle extinction ability in the vertical direction. To verify its reasonableness, we conducted a comparative analysis by obtaining the observation data from the LiDAR located at Southwest Jiao tong University (SWJTU, 104.5 E, 30.73 N). Considering the distance between the LiDAR and meteorological observation stations, Jinquanhe Station (104.3 E, 30.72 N) and Xinduqudishui (104.2 E, 30.78 N) station in Chengdu were used for comparative analysis, and the results are shown in Figure 9. The scatter plots show that the correlation coefficients between the near-ground extinction coefficients calculated by the boundary layer height observed by LiDAR (EXT_vertical (PBL)) and ground-based $PM_{2.5}$ are 0.19 and 0.27, respectively, which are lower than the correlation coefficients between the results calculated based on visibility (EXT_vertical (VIS)) and $PM_{2.5}$. Therefore, the near-ground extinction coefficient calculated by visibility in this study has a higher correlation with $PM_{2.5}$ and is feasible for calculating H_a.

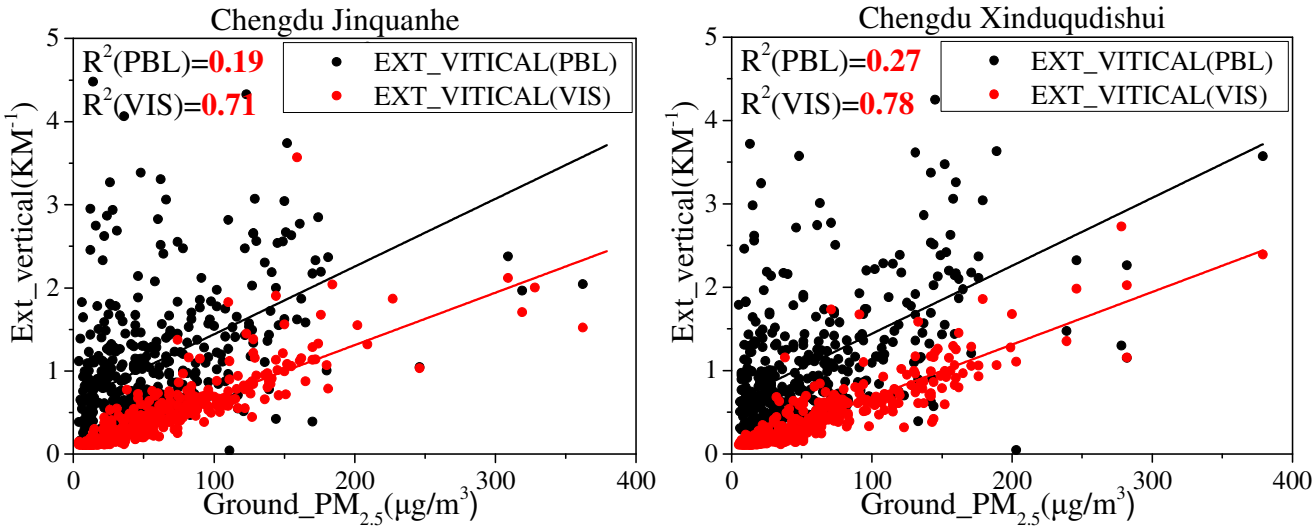

Figure 9. Scatter plots between LiDAR−calculated and visibility−calculated near−ground extinction coefficient and $PM_{2.5}$. The black and red line are LiDAR-calculated and visibility-calculated, respectively.

The study area is located in southwest China, which is less affected by sand and dust so the pollutants in the region are mainly industrial and anthropogenic emissions. Therefore, the defined average mass extinction efficiency is reasonable assuming $PM_{2.5}$ as the main extinction particle in the humidity correction process. The $E_{ext}(RH)$ model was studied experimentally by Kotchenruther [52] for Brazilian aerosols and Magi [55] for South African aerosols. The model is effective for the scattering hygroscopic growth of the carbonaceous aerosol population and can better characterize its variation with humidity. According to the results of the hygroscopic correction fitting (Figure 7), there are some observations that deviate from the fitted curve, but the overall fitting results for the regional stations are good and the fitted curves are relatively smooth, indicating that the adopted $E_{ext}(RH)$ model is feasible.

In addition, when calculating the corrected factor f(90%) (Table 1), no values of relative humidity less than 40% were observed, so their corresponding f(90%) could not be calculated, such as at the Leshan Jiajiangxian station and the Chongqing Guanyinqiao station; this may be related to the humidity environment around the stations. The calculation

results indicate that the aerosol hygroscopic growth capacity is different at different stations in the same month, and it also varies greatly at same stations at different times, so it is necessary to construct a hygroscopic correction factor grid to estimate $PM_{2.5}$ by fitting the hygroscopic growth factor month by month and station by station in the humidity correction, especially for regions with complex topographic conditions.

In this study, the IVW method was used to fuse $PM_{2.5}$ estimated by satellite and simulated by NAQPMS, which bridges the gap area of satellite retrieval and obtains a seamless regional coverage of hour-by-hour $PM_{2.5}$ concentrations (Figures 7 and 8). Compared with other polar-orbiting satellite inversions, the $PM_{2.5}$ concentrations we obtained have a higher temporal–spatial resolution and can help to analyze the variation of pollutants in detail throughout the day. For the urban cluster in Sichuan and Chongqing, which is covered by clouds all year round and has serious pollution in autumn and winter, the fusion results can better present the processes of pollutant migration and dissipation (Figure 8). However, the fusion method is the classical IVW method. With the development of machine learning, much research has applied deep learning to this field and achieved better results, which will be an important research direction at a later stage.

5. Conclusions

Firstly, we used meteorological and environmental ground-based observation data to explore the fitted hygroscopic correction at five different background sites located in Chengdu Linjianglu, Leshan Jiajiangxian, Yibin Xingwenerzhong, Bazhong TongjiangZhongxue, and Chongqing Guanyinqiao. Additionally, the f (90%) was calculated. The results showed that in Sichuan and Chongqing regions with special climatic conditions, the hygroscopic correction factor varies greatly by station and month. Therefore, a hygroscopic correction factor grid with a spatial resolution of 1 km from January to December was constructed by fitting the data from 2017 to 2018 on a site-by-site basis.

Secondly, we verified that the correlation of dry extinction coefficient (σ_{dry}) against $PM_{2.5}$ is improved compared with AOD against $PM_{2.5}$. The hourly near-ground $PM_{2.5}$ concentrations in the study area from 09:00 to 16:00 were estimated by using vertical-humidity method, and the accuracy is verified, with r between 0.69–0.85.

Thirdly, considering that the satellite cannot detect the atmospheric aerosols under the clouds, especially in the Sichuan and Chongqing regions, which have more continuous cloud coverage and gaps in spatial distribution, the advantage of atmospheric model data was fully utilized to obtain seamless coverage results for the region by using the IVW method to fuse $PM_{2.5}$ estimated by satellite and simulated by the atmospheric model. The $PM_{2.5}$ fusion results were used to analyze the processes of aggregation, migration, and dissipation of pollutants.

Finally, we utilized the LiDAR data to demonstrate the reasonableness of this study in discussion. So, the results can effectively provide important supporting data for air pollution control and other works.

Supplementary Materials: The following supporting information can be downloaded at: https://www.mdpi.com/article/10.3390/app12147065/s1, Figure S1. $E_{ext}(RH)$ fitting Leshan Jiajiangxian station. The red solid lines are fitting lines of the scattered dots. Figure S2. $E_{ext}(RH)$ fitting Yibin Xingwenerzhong station. The red solid lines are fitting lines of the scattered dots. Figure S3. $E_{ext}(RH)$ fitting Bazhong Tongjiangzhongxue station. The red solid lines are fitting lines of the scattered dots. Figure S4. $E_{ext}(RH)$ fitting Chongqing Guanyinqiao station. The red solid lines are fitting lines of the scattered dots.

Author Contributions: Q.Z. proposed the method and wrote this paper; H.Z. collected data; Y.G. revised the manuscript. T.X. translated the manuscript. S.L. constructed the model and analyzed data. L.C. revised the manuscript. All authors have read and agreed to the published version of the manuscript.

Funding: This research was funded by the National Natural Science Foundation of China under Grant 42001315, the National Natural Science Foundation of China under Grant 41830109, the National Science and Technology Support Program of China under Grant 2014BAC16B06.

Data Availability Statement: The datasets presented in this study can be found here: http://111.202.113.138:8081/h8/dataquery_h8.jsp; http://106.37.208.233:20035/; https://aeronet.gsfc.nasa.gov/ (accessed on 12 June 2022).

Acknowledgments: All authors would sincerely thank the reviewers and editors for their beneficial, careful, and detailed comments and suggestions for improving the paper.

Conflicts of Interest: The authors declare no conflict of interest.

References

1. Yang, Y.; Guo, Y.F.; Qian, Z.M.; Ruan, Z.L.; Zheng, Y.; Alistair, W.; Ai, S.Q.; Steven, W.H.; Michael, G.V.; Ma, W.J.; et al. Ambient fine particulate pollution associated with diabetes mellitus among the elderly aged 50 years and older in China. *Environ. Pollut.* **2018**, *243*, 815–823. [CrossRef] [PubMed]
2. Hu, Z.Y. Spatial analysis of MODIS aerosol optical depth, $PM_{2.5}$, and chronic coronary heart disease. *Int. J. Health Geogr.* **2009**, *8*, 27. [CrossRef] [PubMed]
3. Tao, M.H.; Chen, L.F.; Su, L.; Tao, J.H. Satellite observation of regional haze pollution over the North China Plain. *J. Geophys. Res. Atmos.* **2012**, *117*, D12203. [CrossRef]
4. Hoff, R.M.; Christopher, S.A. Remote sensing of particulate pollution from space: Have we reached the promised land. *J. Air Waste Manag. Assoc.* **2009**, *59*, 645–675. [CrossRef] [PubMed]
5. Dominici, F.; Peng, R.D.; Bell, M.L.; Pham, L.; McDermott, A.; Zeger, S.L.; Samet, J.M. Fine particulate air pollution and hospital admission for cardiovascular and respiratory diseases. *JAMA* **2006**, *295*, 1127. [CrossRef]
6. Ma, Z.W.; Liu, R.Y.; Liu, Y.; Bi, J. Effects of air pollution control policies on $PM_{2.5}$ pollution improvement in China from 2005–2017: A satellite-based perspective. *Atmos. Chem. Phys.* **2019**, *19*, 6861–6877. [CrossRef]
7. Levy, R.C.; Remer, L.A.; Dubovik, O. Global aerosol optical properties and application to Moderate Resolution Imaging Spectroradiometer aerosol retrieval over land. *J. Geophys. Res. Atmos.* **2007**, *112*, D13210. [CrossRef]
8. Liu, Y.; Park, R.J.; Jacob, D.J.; Li, Q.B.; Vasu, K.; Jeremy, A.S. Mapping annual mean ground-level $PM_{2.5}$ concentrations using multiangle imaging spectroradiometer aerosol optical thickness over the contiguous united states. *J. Geophys. Res. Atmos.* **2004**, *109*, D22206.
9. Donkelaar, V.A.; Martin, R.V.; Brauer, M.K.; Levy, R.; Verduzco, C.; Villeneuve, P.J. Global estimates of ambient fine particulate matter concentrations from satellite-based aerosol optical depth: Development and application. *Environ. Health Perspect.* **2010**, *118*, 847–855. [CrossRef]
10. Donkelaar, V.A.; Martin, R.V.; Brauer, M.; Boys, B.L. Use of satellite observations for long-term exposure assessment of global concentrations of fine particulate matter. *Environ. Health Perspect.* **2014**, *123*, 135–143. [CrossRef]
11. Wang, Z.F.; Chen, L.F.; Tao, J.H.; Zhang, Y.; Su, L. Satellite-based estimation of regional particulate matter (PM) in Beijing using vertical-and-RH correcting method. *Remote Sens. Environ.* **2010**, *114*, 50–63. [CrossRef]
12. Chu, D.A.; Tsai, T.C.; Chen, J.P.; Chang, S.C.; Jeng, Y.J.; Chiang, W.L.; Lin, N.H. Interpreting aerosol lidar profiles to better estimate surface $PM_{2.5}$ for columnar AOD measurements. *Atmos. Environ.* **2013**, *79*, 172–187. [CrossRef]
13. Lin, C.Q.; Li, Y.; Yuan, Z.B.; Alexis, K.H.L.; Li, C.C.; Jimmy, C.H.F. Using satellite remote sensing data to estimate the high-resolution distribution of ground-level $PM_{2.5}$. *Remote Sens. Environ.* **2015**, *156*, 117–128. [CrossRef]
14. Zhang, Y.; Li, Z.Q. Remote sensing of atmospheric fine particulate matter ($PM_{2.5}$) mass concentration near the ground from satellite observation. *Remote Sens. Environ.* **2015**, *160*, 252–262. [CrossRef]
15. Zeng, Q.L.; Chen, L.F.; Zhu, H.; Wang, Z.F.; Wang, X.H.; Zhang, L.; Gu, T.Y.; Zhu, G.Y.; Zhang, Y. Satellite-based estimation of hourly $PM_{2.5}$ concentrations using a vertical-humidity correction method from Himawari-AOD in Hebei. *Sensors* **2018**, *18*, 3456. [CrossRef] [PubMed]
16. Lee, H.J.; Liu, Y.; Coull, B.A.; Schwartz, J.; Koutrakis, P. A novel calibration approach of MODIS AOD data to predict $PM_{2.5}$ concentrations. *Atmos. Chem. Phys.* **2011**, *11*, 7991–8002. [CrossRef]
17. Pu, Q.; Yoo, E.H. Spatio-temporal modeling of $PM_{2.5}$ concentrations with missing data problem: A case study in Beijing, China. *Int. J. Geogr. Inf. Sci.* **2020**, *34*, 423–447. [CrossRef]
18. Ma, Z.W.; Hu, X.F.; Andrew, M.S.; Robert, C.L. Satellite-Based spatiaotemporal trends in $PM_{2.5}$ concentrations China 2004–2013. Environ. *Health Perspect.* **2016**, *124*, 184–192. [CrossRef]
19. Guo, Y.X.; Tang, Q.H.; Gong, D.Y.; Zhang, Z.Y. Estimating ground-level $PM_{2.5}$ concentrations in Beijing using a satellite-based geographically and temporally weighted regression model. *Remote Sens. Environ.* **2017**, *198*, 140–149. [CrossRef]
20. He, Q.Q.; Huang, B. Satellite-based mapping of daily high-resolution ground $PM_{2.5}$ in China via space-time regression modeling. *Remote Sens. Environ.* **2018**, *206*, 72–83. [CrossRef]
21. Liu, Y.; Sarnat, J.A.; Kilaru, V.; Jacob, D.J.; Koutrakis, P. Estimating ground-level $PM_{2.5}$ in the Eastern United States using satellite remote sensing. *Environ. Sci. Technol.* **2005**, *39*, 3269–3278. [CrossRef] [PubMed]

22. Zou, B.; Xu, S.; Sternberg, T.; Fang, X. Effect of land use and cover change on air quality in Urban Sprawl. *Sustainability* **2016**, *8*, 677. [CrossRef]
23. Mitchell, T.M. *Machine Learning*; McGraw-Hill: New York, NY, USA, 1997.
24. Chen, Z.Y.; Zhang, T.H.; Zhang, R.; Zhu, Z.M.; Yang, J.; Chen, P.Y.; Ou, C.Q.; Guo, Y. Extreme gradient boosting model to estimate $PM_{2.5}$ concentrations with missing-filled satellite data in China. *Atmos. Environ.* **2019**, *202*, 180–189. [CrossRef]
25. Liu, Y.; Li, C.Y.; Liu, D.R.; Tang, Y.L.; Barnabas, C.S.; Zhou, Z.H.; Hu, X.; Yang, F.M.; Zhan, Y. Deriving hourly full-coverage $PM_{2.5}$ concentrations across China's Sichuan Basin by fusing multisource satellite retrievals: A machine-learning approach. *Atmos. Environ.* **2022**, *271*, 118930. [CrossRef]
26. Sun, Y.B.; Zeng, Q.L.; Geng, B.; Lin, X.W.; Sude, B.; Chen, L.F. Deep learning architecture for estimating hourly ground-level $PM_{2.5}$ using satellite remote sensing. *IEEE Geosci. Remote Sens. Lett.* **2019**, *16*, 1343–1347. [CrossRef]
27. Fan, W.Z.; Qin, K.; Cui, Y.L.; Li, D.; Bilal, M. Estimation of hourly ground-level $PM_{2.5}$ concentration based on Himawari-8 apparent reflectance. *IEEE Trans. Geosci. Remote Sens.* **2021**, *59*, 76–85. [CrossRef]
28. Zeng, Q.L.; Xie, T.S.; Zhu, S.Y.; Fan, M.; Chen, L.F.; Tian, Y. Estimating the near-ground $PM_{2.5}$ concentration over China based on the CapsNet model during 2018–2020. *Remote Sens.* **2022**, *14*, 623. [CrossRef]
29. Wei, J.; Li, Z.Q.; Sun, L.; Xue, W.H.; Ma, Z.W.; Liu, L.; Fan, T.Y.; Cribb, M. Extending the EOS long-term $PM_{2.5}$ data records since 2013 in China: Application to the VIIRS deep blue aerosol products. *IEEE Trans. Geosci. Remote Sens.* **2022**, *60*, 4100412. [CrossRef]
30. Xu, Q.Q.; Chen, X.L.; Yang, S.B.; Tang, L.L.; Dong, J.D. Spatiotemporal relationship between Himawari-8 hourly columnar aerosol optical depth (AOD) and ground-level $PM_{2.5}$ mass concentration in mainland China. *Sci. Total Environ.* **2021**, *765*, 144241. [CrossRef]
31. Yang, Q.Q.; Yuan, Q.Q.; Yue, L.W.; Li, T.W.; Shen, H.F.; Zhang, L.P. The relationships between $PM_{2.5}$ and aerosol optical depth (AOD) in mainland China: About and behind the spatiotemporal variations. *Environ. Pollut.* **2019**, *248*, 526–535. [CrossRef]
32. Belle, J.H.; Chang, H.H.; Wang, Y.; Hu, X.; Lyapustin, A.; Liu, Y. The potential impact of satellite-retrieved cloud parameters on ground-level $PM_{2.5}$ mass and composition. *Int. J. Environ. Res. Public Health.* **2017**, *14*, 1244. [CrossRef] [PubMed]
33. Bi, J.Z.; Belle, J.H.; Wang, Y.J.; Lyapustin, A.I.; Wildani, A.; Liu, Y. Impacts of snow and cloud covers on satellite-derived $PM_{2.5}$ levels. *Remote Sens. Environ.* **2019**, *221*, 665–674. [CrossRef] [PubMed]
34. Lv, B.; Hu, Y.T.; Chang, H.H.; Russell, A.G.; Bai, Y.Q. Improving the accuracy of daily $PM_{2.5}$ distributions derived from the fusion of ground-level measurements with aerosol optical depth observations, a case study in North China. *Environ. Sci. Technol.* **2016**, *50*, 4752–4759. [CrossRef] [PubMed]
35. Sun, J.; Gong, J.H.; Zhou, J.P. Estimating hourly $PM_{2.5}$ concentrations in Beijing with satellite aerosol optical depth and a random forest approach. *Sci. Total Environ.* **2021**, *762*, 144502. [CrossRef]
36. Li, L.F.; Meredith, F.; Mariam, G.; Frederick, L.; Wu, J.; Nathan, P.; Carrie, B.; Frank, G.; Rima, H. Spatiotemporal imputation of MAIAC AOD using deep learning with downscaling. *Remote Sens. Environ.* **2020**, *237*, 111584. [CrossRef] [PubMed]
37. Chen, B.J.; You, S.X.; Ye, Y.; Fu, Y.Y.; Ye, Z.R.; Deng, J.S.; Wang, K.; Hong, Y. An interpretable self-adaptive deep neural network for estimating daily spatially-continuous $PM_{2.5}$ concentrations across China. *Sci. Total Environ.* **2021**, *768*, 144724. [CrossRef]
38. Bai, K.X.; Li, K.; Guo, J.P.; Chang, N.B. Multiscale and multisource data fusion for full-coverage $PM_{2.5}$ concentrantion mapping: Can spatial pattern recognition come with modeling accuracy? *ISPRS J. Photogramm. Remote Sens.* **2022**, *184*, 31–44. [CrossRef]
39. Liao, T.T.; Gui, K.; Jiang, W.T.; Wang, S.G.; Wang, B.H.; Zeng, Z.L.; Che, H.Z.; Wang, Y.Q.; Sun, Y. Air stagnation and its impact on air quality during winter in Sichuan and Chongqing, southwestern China. *Sci. Total Environ.* **2018**, *635*, 576–585. [CrossRef]
40. Tao, J.; Zhang, L.M.; Engling, G.; Zhang, R.J.; Yang, Y.H.; Cao, J.J.; Zhu, C.S.; Wang, Q.Y.; Luo, L. Chemical composition of $PM_{2.5}$ in an urban environment in Chengdu, China: Importance of springtime dust storms and biomass burning. *Atmos. Res.* **2013**, *122*, 270–283. [CrossRef]
41. Yang, F.K.; Wang, Y.; Tao, J.H.; Wang, Z.F.; Fan, M.; Gerrit, D.L.; Chen, L.F. Preliminary investigation of a new AHI aerosol optical depth (AOD) retrieval algorithm and evaluation with multiple source AOD measurements in China. *Remote Sens.* **2018**, *10*, 748. [CrossRef]
42. Husar, R.B.; Husar, J.D.; Martin, L. Distribution of continental surface aerosol extinction based on visual range data. *Atmos. Environ.* **2000**, *34*, 5067–5078. [CrossRef]
43. Levy, R.C.; Remer, L.A.; Mattoo, S.; Vermote, E.F.; Yoram, J.F. Second-generation operational algorithm: Retrieval of aerosol properties over land from inversion of Moderate Resolution Imaging Spectroradiometer spectral reflectance. *J. Geophys. Res. Atmos.* **2007**, *112*, D13211. [CrossRef]
44. McHardy, T.M.; Zhang, J.; Reid, J.S.; Miller, S.D.; Hyer, E.J.; Kuehn, R.E. An improved method for retrieving nighttime aerosol optical thickness from the VIIRS Day/Night Band. *Atmos. Meas. Tech.* **2015**, *8*, 4773–4783. [CrossRef]
45. Wang, Z.; MAEDA, T.; Hayashi, M.; Hsiao, L.F.; Liu, K.Y. A nested air quality prediction modeling system for urban and regional scales: Application for high-ozone episode in Taiwan. *Water Air Soil Pollut.* **2001**, *130*, 391–396. [CrossRef]
46. Wang, Z.; Pan, X.L.; Uno, I.; Chen, X.S.; Yamamoto, S.; Zheng, H.T.; Li, J.; Wang, Z.F. Importance of mineral dust and anthropogenic pollutants mixing during a long-lasting high PM event over East Asia. *Environ. Pollut.* **2018**, *234*, 368–378. [CrossRef]
47. Wang, Q.X.; Zeng, Q.L.; Tao, J.H.; Sun, L.; Zhang, L.; Gu, T.Y.; Wang, Z.F.; Chen, L.F. Estimating $PM_{2.5}$ concentrations based on MODIS AOD and NAQPMS data over Beijing-Tianjin-Hebei. *Sensors* **2019**, *19*, 1207. [CrossRef]
48. Koelemeijer, R.; Homan, C.; Matthijsen, J. Comparison of spatial and temporal variations of aerosol optical thickness and particulate matter over Europe. *Atmos. Environ.* **2006**, *40*, 5304–5315. [CrossRef]

49. Koschmieder, H. Theorie der horizontalen sichtweite II: Kontrast und sichtweite. *Beiträge Phys. Freien Atmosphäre* **1925**, *12*, 171–181.
50. Wan, H.Y.; Dong, X.B.; Liu, S.Y.; Pu, J.P. Analysis on aerosol scale height based on aircraft observation and MODIS products over North China. *J. Meteorol. Sci.* **2016**, *36*, 655–660.
51. Zhang, Z.Y.; Wu, W.L.; Wei, J.; Song, Y.; Yan, X.D.; Zhu, L.D.; Wang, Q. Aerosol optical depth retrieval from visibility in China during 1973–2014. *Atmos. Environ.* **2017**, *171*, 38–48. [CrossRef]
52. Kotchenruther, R.A.; Hobbs, P.V. Humidification factors of aerosols from biomass burning in Brazil. *J. Geophy. Res. Atmos.* **1988**, *103*, 32081–32089. [CrossRef]
53. Ma, Z. Study on Spatiotemporal Distributions of $PM_{2.5}$ in China Using Satellite Remote Sensing. Ph.D. Thesis, Nanjing University, Nanjing, China, 2015.
54. Wang, Z.F.; Chen, L.F.; Tao, J.H.; Liu, Y.; Hu, X.F.; Tao, M.H. An empirical method of RH correction for satellite estimation of ground-level PM concentrations. *Atmos. Environ.* **2014**, *95*, 71–81. [CrossRef]
55. Magi, B.I.; Hobbs, P.V. Effects of humidity on aerosols in southern Africa during the biomass burning season. *J. Geophys. Res. Atmos.* **2003**, *108*, 8495. [CrossRef]